nature portfolio

https://doi.org/10.1038/s41586-023-06360-6

Supplementary information

Realizing spin squeezing with Rydberg interactions in an optical clock

In the format provided by the authors and unedited

Supplementary Information: Realizing spin squeezing with Rydberg interactions in an optical clock

William J. Eckner, Nelson Darkwah Oppong, Alec Cao, Aaron W. Young, William R. Milner, John M. Robinson, Jun Ye, Adam M. Kaufman
JILA, University of Colorado and National Institute of Standards and Technology, and Department of Physics, University of Colorado, Boulder, Colorado 80309, USA
(Dated: May 30, 2023)

CONTENTS

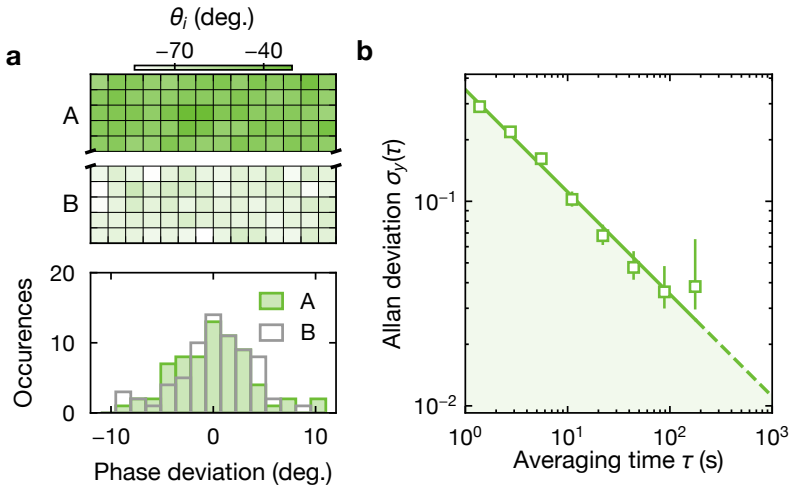

FIG. S1. **Characterization of tweezer phase shifting homogeneity and stability. a**, Site-resolved Ramsey fringe phases for two $N = 5 \times 14$ subarrays with the phase shifting protocol described in Fig. 4a applied during the dark time to ensemble A. For each site i, θ_i is obtained by fitting $P_i \sim \sin(\theta_L + \theta_i)$. The lower panel shows a histogram of the difference of θ_i from the relevant average subarray phase θ_A and θ_B. The standard deviation of the θ_i distribution for ensemble A (B) is 3.8° (3.6°). **b**, Overlapping Allan deviation for the applied phase shift. The laser phase θ_L is set so that $(P_A + P_B)/2 \approx 1/2$ on average. The deviation is computed for $2d_z^{(AB)}/(\phi C)$; here, ϕ and C are computed from the measurement in **a**, with $\phi = \theta_A - \theta_B = 33.2(1.3)°$ and $C = 0.971(2)$ obtained from averaging the contrasts of subarrays A and B.

I. CHARACTERIZATION OF LOCAL $\hat{\sigma}_z$ OPERATIONS

In order to minimize added technical noise, the local light-shifting protocol presented in Fig. 4a and the Methods should be the same across the atom array (spatially homogeneous), and consistent between different experiments (temporally homogeneous). To characterize spatial homogeneity, we measure site-resolved Ramsey fringes, and analyze the distribution of fitted phases, shown in Fig. S1a. We benchmark the temporal homogeneity of the the protocol by performing an atom-atom stability measurement for 5×14 subarrays with the tweezers applied during a short dark time. Because the ensembles are phase shifted relative to each other, the phase of the final $\pi/2$-pulse is chosen such that the average $S_z^{(A)} + S_z^{(B)} = 0$. Results of this measurement are shown in S1b. We note that any ellipse measurements utilizing $\hat{\sigma}_z$ operations alternate experimental shots where the Rydberg laser is applied or not, and thereby interleave data acquisition for the SSS and CSS. As a result, the SSS and CSS should experience similar systematic effects, such as any slow residual drift of the applied phase offset between subarrays.

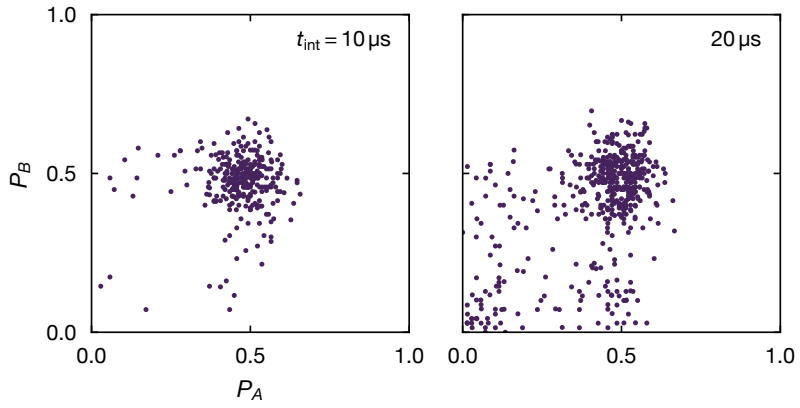

FIG. S2. **Emerging collective effects at late times.** As in the main text, we denote the excitation fraction P_A, P_B for subarray A, B, respectively. In the left (right) panel we parametrically plot the excitation fractions P_A and P_B, measured after a total interaction time $t_{\rm int} = 10\,\mu$s ($20\,\mu$s). For this measurement, we determine the excitation fraction immediately after the second Rydberg-interaction pulse (see Fig. 1c in the main text), and with two $N = 5 \times 14$ subarrays.

II. SIGNATURES OF COLLECTIVE DISSIPATION

In addition to altered unitary dynamics, observations in larger subarrays might be impacted by non-unitary dynamics in the form of collective dissipation [1–5]. For example, when increasing the interaction time to $t_{\rm int} \geq 10\,\mu$s – a regime beyond the typical optima for preparing SSSs – signs of a bimodal distribution emerge in the atomic excitation fraction for two $N = 5 \times 14$ subarrays. By plotting the excitation fractions P_A, P_B for two subarrays A and B, respectively, as shown in Fig. S2, we can further see a bimodal distribution emerge in P_A, even when controlling for P_B (and vice-versa). This observation indicates the presence of collective effects and, therefore, appears to be consistent with the presence of collective dissipation phenomena, which have been studied in similar Rydberg-atom-array platforms [1–5].

III. DERIVATION OF QPN AND ξ_W^2

In this section, we derive expressions for quantum projection noise (QPN) and the Wineland parameter presented in the main text. To begin, S_z/N for two ensembles A and B in a Ramsey-style measurement will be given by

$$\begin{aligned} \frac{S_z^{(A)}}{N} &= \frac{C}{2}\sin(\theta + \pi/2) + y_A \\ \frac{S_z^{(B)}}{N} &= \frac{C}{2}\sin(\theta + \phi + \pi/2) + y_B \end{aligned} \tag{S.1}$$

where we refer to θ as the atom-laser phase, and ϕ as the differential phase. We have furthermore assumed that both ensembles have the same contrast $0 \leq C \leq 1$, but potentially

different offsets $C-1 \leq 2\,y_A, 2\,y_B \leq 1-C$. Finally, N refers to the atom number in each ensemble, which we take to be equal ($N_A = N_B = N$).

We are interested in the noise in the measurement of $\hat{d}_z^{(AB)}$, as defined in the main text. To motivate this decision, we show that this provides a measurement of the differential phase ϕ. Writing out the expectation value of $\hat{d}_z^{(AB)}$ gives

$$d_z^{(AB)} = \frac{S_z^{(A)} - S_z^{(B)}}{N} = \frac{C}{2}[\sin(\theta + \pi/2) - \sin(\theta + \phi + \pi/2)] + (y_A - y_B). \tag{S.2}$$

Taylor-expanding about the point $(\theta, \phi) = (\pi/2, 0)$ yields

$$d_z^{(AB)} \approx \frac{C}{2}\phi + (y_A - y_B). \tag{S.3}$$

The phase uncertainty of our measurement will then be

$$\Delta\phi = \Delta\hat{d}_z^{(AB)} \left| \frac{\mathrm{d}d_z^{(AB)}}{\mathrm{d}\phi} \right|^{-1} = \frac{2\Delta\hat{d}_z^{(AB)}}{C}. \tag{S.4}$$

We now define the quantum-projection-noise limit as the variance of an ideal (contrast $C = 1$) coherent spin state $|\mathrm{CSS}\rangle$

$$|\mathrm{CSS}\rangle = |\theta + \phi\rangle_A \otimes |\theta\rangle_B \tag{S.5}$$

where

$$\begin{aligned} |\theta\rangle_A &= \bigotimes_{i=0}^{N-1} [e^{-i\theta/2}\,|e\rangle_i + e^{i\theta/2}\,|g\rangle_i]/\sqrt{2} \\ |\theta+\phi\rangle_B &= \bigotimes_{j=0}^{N-1} [e^{-i(\theta+\phi)/2}\,|e\rangle_j + e^{i(\theta+\phi)/2}\,|g\rangle_j]/\sqrt{2}\,. \end{aligned} \tag{S.6}$$

and i (j) indexes atoms in ensemble A (B). Using the notation presented in the main text,

$$\sigma^2_{\mathrm{QPN}} = \langle \mathrm{CSS}|\,[\hat{d}_z^{(AB)}]^2\,|\mathrm{CSS}\rangle - [\langle \mathrm{CSS}|\,\hat{d}_z^{(AB)}\,|\mathrm{CSS}\rangle]^2 \tag{S.7}$$

$$= \frac{1}{2N}\,. \tag{S.8}$$

From this, the standard quantum limit on our estimation of ϕ is

$$(\Delta\phi)_{\mathrm{SQL}} = \sqrt{\frac{2}{N}}\,. \tag{S.9}$$

Next, we derive an expression for the squeezing parameter, which is typically defined in the context of a Ramsey measurement with a single ensemble of N atoms and an atom-laser phase θ as [6]

$$\xi_\theta^2 = \frac{(\Delta\theta)^2}{(\Delta\theta)^2_{\mathrm{SQL}}}\,. \tag{S.10}$$

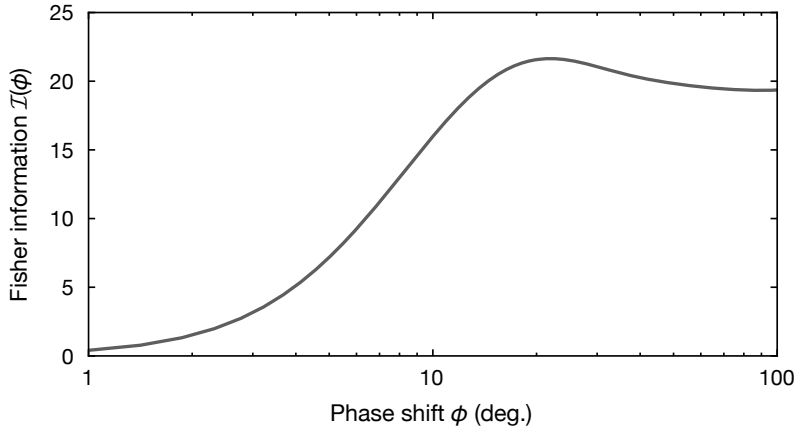

FIG. S3. **Measurement sensitivity of ellipse fitting.** Here, we consider a variable phase shift ϕ between two subarrays and quantify the measurement sensitivity using the classical Fisher information (solid gray line). Here, a coherent spin state with contrast $C = 0.95$ is considered.

Here, $\Delta\theta$ is the uncertainty in the measured atom-laser phase, and

$$(\Delta\theta)_{\mathrm{SQL}} = \sqrt{\frac{1}{N}}\,. \tag{S.11}$$

In the context of our differential measurement of ϕ, we therefore define the parameter ξ_ϕ^2 as

$$\xi_\phi^2 = \frac{(\Delta\phi)^2}{(\Delta\phi)^2_{\mathrm{SQL}}} = \frac{\sigma_\alpha^2}{C^2}\frac{1}{\sigma^2_{\mathrm{QPN}}} \tag{S.12}$$

where the angle α sets the measurement quadrature. The Wineland parameter ξ_W^2 in the main text is then

$$\xi_W^2 = \left[\xi_\phi^2\right]_{\mathrm{min}} = \frac{\sigma^2_{\mathrm{min}}}{C^2}\frac{1}{\sigma^2_{\mathrm{QPN}}} \tag{S.13}$$

where 'min' refers to the minimum over α.

IV. FISHER INFORMATION OF CSS FOR ELLIPSE FITTING

In Fig. S3, we present a calculation of the Fisher information in a coherent spin state (CSS) for measuring ϕ in an ellipse-fitting protocol. In this calculation, we consider the probability mass function

$$f_{\mathrm{CSS}}\left(p_A, p_B|\phi, C, y_0\right) = f\left(p_A, p_B|\phi, C, y_0, \vec{\zeta} = (1,1)\right) \tag{S.14}$$

where the function $f\left(p_A, p_B|\phi, C, y_0, \vec{\zeta}\right)$ is defined in the Methods. The parameter regime in which $\vec{\zeta} = (1,1)$ corresponds to a binomial model, which captures the statistics of uncorrelated atoms in a CSS. The Fisher information for a measurement of ϕ with this probability

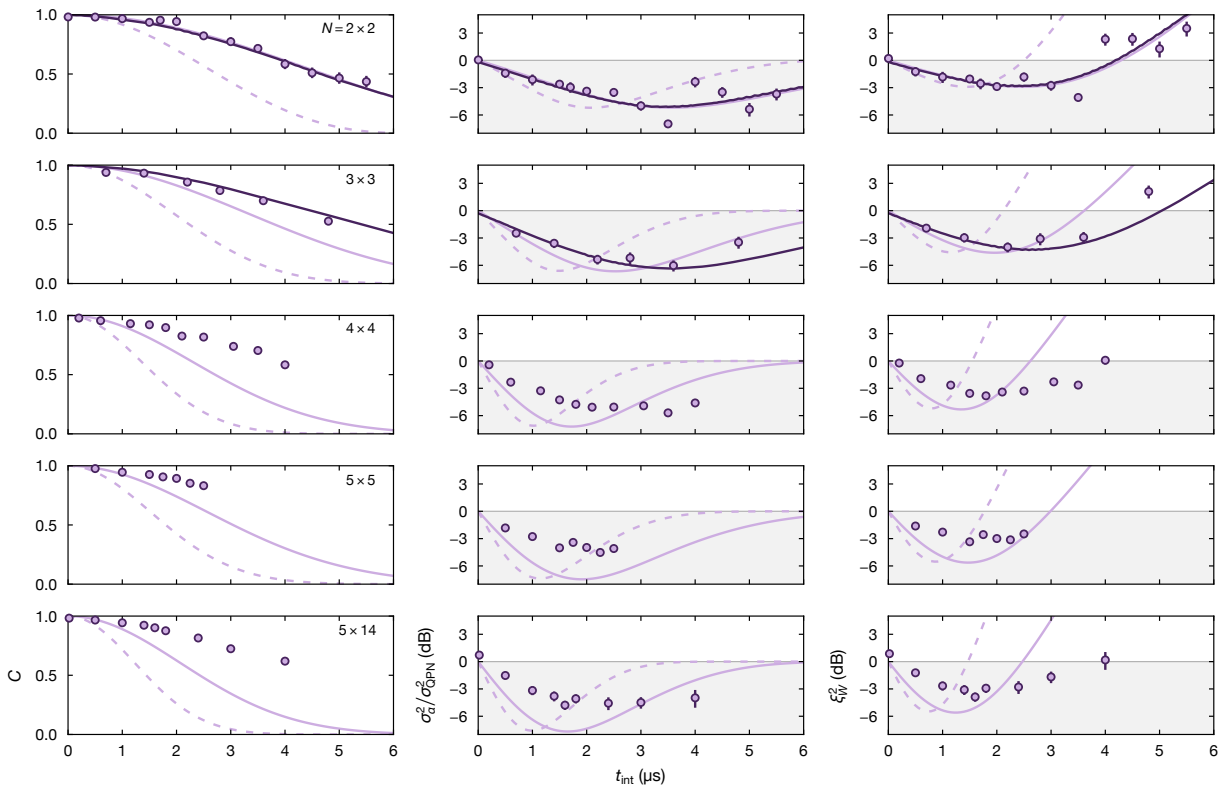

FIG. S4. **Squeezing dynamics in the experiment and numerical simulations.** Here, we show experimental measurements (purple circles) for the contrast C (left column), variance reduction $\sigma_\alpha^2/\sigma_{\mathrm{QPN}}^2$ (center column), and the Wineland parameter ξ_W^2 (right column). From top to bottom, the atom number increases from $N = 2 \times 2 = 4$ to $5 \times 14 = 70$ in each row. Dark purple lines correspond to an exact-diagonalization calculation (see Methods) for the parameters in the experiment. Solid light purple lines show the theoretical predictions from weak-dressing [7] using $\tilde{V}_0$ and $\tilde{R}_b$ from the fit shown in Fig. 1b of the main text. Dashed purple lines correspond to the same theory, but with $V_0 = \hbar\beta^3\Omega_r$ and $R_b = |C_6/(2\Delta)|^{(1/6)}$.

distribution is then

$$\mathcal{I}_{\mathrm{CSS}}(\phi_0) = \sum_{p_A=0/N}^{N/N} \sum_{p_A=0/N}^{N/N} \left\{ \frac{\partial}{\partial\phi} \log\left[f_{\mathrm{CSS}}(p_A, p_B|\phi, C, y_0)\right]\Big|_{\phi=\phi_0} \right\}^2 f_{\mathrm{CSS}}(p_A, p_B|\phi_0, C, y_0) \ . \tag{S.15}$$

In Fig. S3, we plot $\mathcal{I}_{\mathrm{CSS}}(\phi)$ versus ϕ for the parameters $C = 0.95$, $y_0 = 0.5$, which are representative of typical experimental values.

V. COMPARISON OF DYNAMICS IN THE EXPERIMENT WITH THEORY

In this section, we directly compare the dynamics observed in the experiment to theoretical predictions from numerical simulations. For the weak dressing theory, as outlined in the

Methods section of the main text, we choose two different approaches. In the first approach, we use the values of $\tilde{V}_0$ and $\tilde{R}_b$ obtained from the fit shown in Fig. 1b with a minor rescaling to adjust for slightly different parameters in each measurement. In the second approach, we calculate $V_0 = \hbar\beta^3\Omega_r$ and $R_b = |C_6/(2\Delta)|^{(1/6)}$ from Ω_r, Δ, and C_6.

In addition to the weak-dressing theory, we also consider a *strong-dressing theory* which corresponds to an exact-diagonalization calculation of the full three-level Rydberg Hamiltonian. This procedure is motivated by the fact that we operate with a relatively large $\beta \approx 0.25$, which we empirically find to maximize the achievable squeezing. In this regime, the two-body interaction strengths V_{ij} deviate from the predictions of weak dressing, and collective interactions can play an elevated role [8, 9]. Such effects could cause unitary dynamics in the system that are not captured by Eq. (1).

For small atom numbers ($N \leq 9$ in this work), the full three-level system ($|g\rangle$, $|e\rangle$, and $|r\rangle$) is simulated via exact diagonalization. In this case, the Hamiltonian describing the off-resonantly driven Rydberg system is:

$$\frac{\hat{H}_3}{\hbar} = \frac{\Omega_r(t)}{2}\sum_i \left(|e\rangle\langle r|_i + \text{h.c.}\right) + \Delta(t)\sum_i |r\rangle\langle r|_i + \sum_{i<j}\frac{C_6}{r_{ij}^6}|r\rangle\langle r|_i |r\rangle\langle r|_j + \frac{\Omega_c(t)}{2}\sum_i \left(|g\rangle\langle e|_i + \text{h.c.}\right). \tag{S.16}$$

We implement a step function for the clock Rabi frequency $\Omega_c(t)$ and a linear ramp both for the detuning $\Delta(t)$ and Rydberg Rabi frequency $\Omega_r(t)$ to model the experimental procedures (see *Rydberg drive and parameters* in the Methods section of the main text). These linear ramps have a duration of 225 ns, and are discretized with a step size of 6.5 ns in our simulations. The initial state is given by $|\psi_0\rangle = |gg\ldots g\rangle$ and we time-propagate it under $e^{-i\hat{H}_3 t/\hbar}$ using the software library `quspin` [10]. From the final state, the relevant quantities C, $\sigma_\alpha^2/\sigma_{\text{QPN}}^2$, and ξ_W^2 are determined. This calculation assumes perfect clock rotations and does not contain any free parameters, i.e., the relevant parameters of $\hat{H}_3$ are determined independently (see *Rydberg drive and parameters* in the Methods section of the main text).

For the exact-diagonalization calculation (see dark purple lines in Fig. S4), we generally find good qualitative agreement between experiment and theoretical prediction for the numerically accessible subarray sizes $N = 2\times 2$ and 3×3. For the first weak-dressing approach (see light purple lines in Fig. S4), we find similarly good agreement for $N = 2\times 2$, but for larger subarray sizes the dynamical time scale becomes significantly faster than the one observed in the experiment. Moreover, the theoretically predicted maximum squeezing $1/\xi_W^2$ becomes significantly larger than the experimentally observed one. For the second weak-dressing approach (see dashed light purple lines in Fig. S4), the theoretically predicted dynamics are even faster since $\tilde{V}_0 < V_0$ which sets the characteristic time scale of the system [7].

[1] J. Zeiher, R. Van Bijnen, P. Schauß, S. Hild, J.-y. Choi, T. Pohl, I. Bloch, and C. Gross, Many-body interferometry of a Rydberg-dressed spin lattice, Nat. Phys. **12**, 1095 (2016).

[2] T. Boulier, E. Magnan, C. Bracamontes, J. Maslek, E. Goldschmidt, J. Young, A. Gorshkov, S. Rolston, and J. V. Porto, Spontaneous avalanche dephasing in large Rydberg ensembles, Physical Review A **96**, 053409 (2017).

[3] E. Guardado-Sanchez, B. M. Spar, P. Schauss, R. Belyansky, J. T. Young, P. Bienias, A. V. Gorshkov, T. Iadecola, and W. S. Bakr, Quench Dynamics of a Fermi Gas with Strong Nonlocal Interactions, Phys. Rev. X **11**, 021036 (2021).

[4] J. T. Young, T. Boulier, E. Magnan, E. A. Goldschmidt, R. M. Wilson, S. L. Rolston, J. V. Porto, and A. V. Gorshkov, Dissipation-induced dipole blockade and antiblockade in driven Rydberg systems, Physical Review A **97**, 023424 (2018).

[5] L. Festa, N. Lorenz, L.-M. Steinert, Z. Chen, P. Osterholz, R. Eberhard, and C. Gross, Blackbody-radiation-induced facilitated excitation of Rydberg atoms in optical tweezers, Phys. Rev. A **105**, 013109 (2022).

[6] D. J. Wineland, J. J. Bollinger, W. M. Itano, F. L. Moore, and D. J. Heinzen, Spin squeezing and reduced quantum noise in spectroscopy, Phys. Rev. A **46**, R6797 (1992).

[7] L. I. R. Gil, R. Mukherjee, E. M. Bridge, M. P. A. Jones, and T. Pohl, Spin Squeezing in a Rydberg Lattice Clock, Phys. Rev. Lett. **112**, 103601 (2014).

[8] J. Honer, H. Weimer, T. Pfau, and H. P. Büchler, Collective Many-Body Interaction in Rydberg Dressed Atoms, Phys. Rev. Lett. **105**, 160404 (2010).

[9] N. Henkel, R. Nath, and T. Pohl, Three-Dimensional Roton Excitations and Supersolid Formation in Rydberg-Excited Bose-Einstein Condensates, Phys. Rev. Lett. **104**, 195302 (2010).

[10] P. Weinberg and M. Bukov, QuSpin: a Python package for dynamics and exact diagonalisation of quantum many body systems part I: spin chains, SciPost Phys. **2**, 003 (2017).